

IMPACT OF VARIABLE BATH CHEMISTRY AND WETTING ON GAS BUBBLE FLOW IN ALUMINIUM ELECTROLYSIS CELLS

Kristian Etienne Einarsrud¹, Ingo Eick², Peter J. Witt³, Asbjørn Solheim⁴, Yuqing Feng³

¹Sør Trøndelag University College (HiST), 7004 Trondheim, Norway

²Hydro Aluminium Deutschland GmbH, 41468 Neuss, Germany

³CSIRO Mineral Resources Flagship, 3169 Melbourne, Australia

⁴SINTEF Materials and Chemistry, 7465 Trondheim, Norway

Keywords: Hall-Héroult cell, bubble dynamics, bath properties, electrolyte chemistry

Abstract

A phenomenological model for the creation and transport of anodic gas bubbles in Hall-Héroult cells has been developed, following a multiscale approach. The essential features of the modelling framework are reviewed and discussed in the present paper. The model covers the generation of molecular gas species through Faradays law, subsequent bubble nucleation, and the evolution of macroscopic bubbles which are treated by a volume of fluid model. Recently, the modelling framework has been extended to include several complex phenomena such as surface tension and wetting, bath chemistry, and variable flow properties.

The modelling framework has currently been applied to a laboratory scale electrolysis cell setup. The results demonstrate that the essential properties are well represented over a large range of experimental conditions by the proposed approach.

Introduction

The Hall-Héroult process is the dominant industrial scale technology for reducing alumina powder to primary aluminium metal. Reduction cell performance depends upon several complex physical processes that occur in the cell, including electrochemical, electro-magnetic, hydrodynamic and heat- and mass transfer processes.

Aluminium reduction cells operate in a harsh environment, which, along with restricted access make measurements on operating cells challenging. In order to develop new cells and to improve the performance of existing cells, new tools are needed. Moxnes et al. [1] described how optimized alumina feeding can improve performance. However, experimentation is very costly and time consuming. Mathematical models can provide a tool to understand and explore how changes affect performance (Gusberty et al. [2]). Validated mathematical models can thus provide a more efficient means of achieving improved cell performance than through experimentation.

Over the last few years, considerable effort has been

made to develop detailed simulation tools in order to better assess the behavior of fluid flow and alumina distribution in the narrow region between the anode and cathode in Hall-Héroult cells; the ACD. Owing to the large span of physical scales present in reduction cells, ranging from several meters when considering the whole cell to a fraction of a millimeter when considering bubble nuclei, it is currently not possible to envisage a single model allowing for a simultaneous treatment of all relevant scales. Consequently, researchers have focused on either macroscopic models, aiming to describe global features in a single cell, or micro- to mesoscale models, aiming to describe local features on a single anode or a portion thereof.

An extensive macroscale modelling framework has been developed by Feng et al. [3]-[5] and Witt et al. [6], aiming to describe the global flow fields and transport of alumina in a full cell, based on a steady state Eulerian-Eulerian bath-bubble flow model. This modelling framework has recently been extended by Witt et al. [7] by including six chemical species so as to more accurately represent the underlying electro-chemistry.

As a consequence of aiming for a global and long term description of flow and specie distributions, the above modelling framework does not resolve detailed features such as for instance dynamic bubble interfaces, coalescence and localized effects due to bubble screening. Instead, the global approach relies upon semi-empirical closure laws, based on temporal and volume averaged values of fields of relevance. These fields are typically obtained from experiments, for instance water model experiments, but could in principle also be deduced from dedicated mesoscale simulations, in which the phenomena in question are resolved.

In parallel to the macro scale developments, progress has been made on such a mesoscale approach, based upon the work of Einarsrud [8] and Einarsrud et al. [9],[10], with the ultimate goal of providing a numerical laboratory from which relevant closure relations can be deduced.

In the current paper, recent progress in the mesoscale approach is described, with focus on the importance of

wetting and surface phenomena on the anode, inspired by recent experimental studies by Simonsen et al. [11]. Following a verification based on lab scale electrolysis experiments conducted by Eick et al. [12], the influence of the bath chemistry model proposed by Witt et al. [7] upon the mesoscale approach is assessed.

Model description

The modelling framework proposed in [8] is a multiscale and multifield approach, aiming to fully resolve the behaviour of macroscopic anodic bubbles (down to a few millimeters), while phenomena occurring at smaller scales (for instance nucleation of small bubbles) is treated by means of applicable sub-grid models. The proposed modelling framework consists of five field classes, as shown in figure 1.

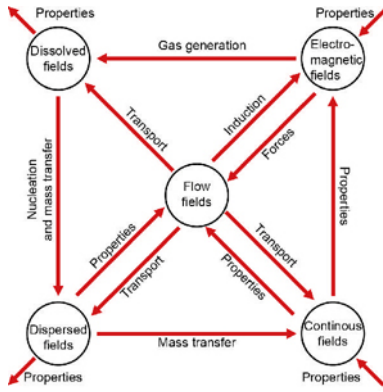


Figure 1: Overview of fields in modelling framework and their interaction.

Taking CO_2 as an example, it is produced on the anode surface owing to the presence of an electrical current, resulting in a field of dissolved CO_2 in close proximity of the anode. As concentrations amount to saturation, CO_2 bubbles nucleate and form a dispersed bubble field, which evolves by means of coalescence and mass transfer. Upon reaching a critical volume fraction, the dispersed bubble field is converted to a continuous (fully resolved) field.

The outer fields depicted in figure 1 are transported and coupled to the flow fields, while the behaviour of the electromagnetic fields (i.e. current density) and flow fields are coupled to the various material properties (e.g. electrical conductivity and viscosity) determined by the relative concentrations of dissolved species and dispersed and continuous gas fields. Evidently, the proposed modelling framework is capable of dynamically predicting for instance anodic voltage oscillations, which arise due to the quasi-periodic formation and release of anodic gas bubbles.

Details regarding each of the fields can be found in the

literature, cf. for instance [9], but for the sake of completeness, a brief overview of each of the nodes shown in figure 1 is given in the following sections.

Electromagnetic fields

The principal driving force for gas evolution is the current density \mathbf{j} , which drives the production of dissolved CO_2 as of Faraday's equations. The current density is obtained by solving a Laplace equation for the electrical potential ϕ ;

$$\nabla \sigma \nabla \phi = 0, \quad (1)$$

where σ is the electrical conductivity, depending upon local specie- and gas concentrations.

Dissolved fields

Seven separate species are considered in the current framework; Al_2O_3 , NaF , AlF_3 , $\text{Na}_2\text{Al}_2\text{O}_2\text{F}_4$, $\text{Na}_2\text{Al}_2\text{OF}_6$, Na^+ and CO_2 . The first six correspond to those proposed in [7], aiming to represent the principal components of an alumina-cryolite bath, while CO_2 is modelled as a dissolved specie *in the bath*, as argued for in [10]. The behaviour of all species are treated by the generic advection-diffusion equation

$$\frac{\partial \rho_b Y_i}{\partial t} + \nabla \cdot (\mathbf{u} \rho_b Y_i - \rho_b \mathcal{D}_i^e \nabla Y_i) = S_i^p - S_i^c, \quad (2)$$

on a mass fraction Y_i basis, where ρ_b is the bath density, \mathbf{u} is the local fluid velocity, \mathcal{D}_i^e is the effective diffusivity (including turbulent diffusion where applicable) and S_i^p and S_i^c respectively represent source and sink terms due to production and consumption of the i -th specie, for instance due to electrochemical reactions. Relevant reaction schemes and details regarding the form of the source terms can be found in [7] and [9].

Dispersed fields

The dispersed bubble field is concerned with the small scale bubbles, typically ranging from a diameter of 0.4 mm and up to sizes dictated by the numerical resolution in proximity of the anode, typically 1-3 mm. As the dispersed bubbles are not resolved, they are modelled by means of a discrete population balance approach, with conservation equation for the number density n_i of the i -th bubble size class

$$\frac{\partial n_i}{\partial t} + \nabla \cdot (f(\mathbf{u}) n_i - \mathcal{D}_i^{PBM} \nabla n_i) = b_i - d_i, \quad (3)$$

where $f(\mathbf{u})$ is an advection function, \mathcal{D}_i^{PBM} is a diffusion coefficient and b_i and d_i respectively represent birth and death rates for the given bubble class. The birth and death rates include bubble nucleation, mass transfer and coalescence, considering both sub-grid-sub-grid interactions and sub-grid-resolved bubble interactions. Details can be found in [9].

Continuous and flow fields

The continuous (resolved) fields in the current framework are treated by means of the Volume of Fluid (VOF) method, allowing for direct simulations of the complex bubble topology present on the anode surface. In the VOF-method, the evolution of the the k -th continuous field with density ρ_k is governed by a phase fraction equation of the form

$$\frac{\partial}{\partial t} (\alpha_k \rho_k) + \nabla \cdot (\alpha_k \rho_k \mathbf{u}) = S_k^\alpha, \quad (4)$$

where S_k^α is a source term originating from interactions with sub-grid entities. A single flow field is shared between the phases, governed by the incompressible Navier-Stokes equations, with additional source terms relating to surface tension as of the continuum surface stress model, cf. Lauffaurie et al. [13].

Turbulence is modelled in the continuous phases by means of the realizable k- ϵ -model (Shih et al. [14]), with enhanced wall treatment.

Properties

The observed voltage oscillations in Hall-Héroult cells are due to the quasi-periodic formation and detachment of gas bubbles, which have negligible electrical conductivity compared to the cryolite bath. Evidently, this property is of fundamental interest for any realistic simulation of the system considering gas production, as gas production is driven by the local current density. The electrical conductivity of the continuous domain, σ , is in the current framework modelled by an arithmetic average

$$\sigma = \sigma_g \alpha_g + \bar{\sigma}_b (1 - \alpha_g), \quad (5)$$

where subscripts g and b respectively represent (continuous) gas and bath phases. $\bar{\sigma}_b$ represents the *mean* bath conductivity, modelled by the Bruggeman equation

$$\bar{\sigma}_b = \sigma_g \alpha_g^D + \sigma_b (1 - \alpha_g^D)^{3/2}, \quad (6)$$

where α_g^D is the volume fraction of *dispersed* gas bubbles and $\bar{\sigma}_b$ is the conductivity of the bath at a given composition Y_i .

Parametric studies, cf. [8] and [11], have revealed a strong dependency of surface tension and wetting conditions upon anodic bubble evolution. Consequently, the influence of bath chemistry upon these properties are investigated further in the current work.

Surface tension, γ , is assumed to follow the correlation proposed by Thonstad et al. [15], while the bath-gas contact angle, θ_{bg} ($^\circ$) is assumed to follow the correlation

$$\theta_{bg} = 120 - 0.1 \ln [15wt(\text{Al}_2\text{O}_3)] \cdot (100 - wt(\text{Al}_2\text{O}_3)), \quad (7)$$

where $wt(\text{Al}_2\text{O}_3)$ is the (effective) weight% of alumina (consisting of alumina and both oxyfluoride species) based upon the experimental data of Dorward [16].

Realization of framework

The proposed framework has been fully realized in ANSYS FLUENT R14.5 [17], utilizing the user defined function and -scalar functionality to extend the existing features to the current requirements. Details regarding the implementation and recommended solver settings can be found in [8].

Experiments

Simulations are validated against lab scale electrolysis experiments described in [12]. In the experiments a 100 by 100 mm anode was made from industrial (anode) carbon and placed in a cylindrical graphite lined crucible lined with Si_3N_4 with inner diameter 230 mm. The anode was fixed to a steel rod so that the anode-cathode distance could be varied. Moreover, two of the anode sides were fitted with Si_3N_4 -plates in order to force gas bubbles to escape in a preferred direction. Finally, the complete cell could be tilted, allowing for studies of gas bubble evolution on inclined anode surfaces. The anode was connected to an external power supply, allowing for current densities up to 1.22 A/cm². Initially, 6.7 kg of industrial bath was melted and alumina was added regularly maintaining concentrations close to that of saturation.

Electrolysis was performed under various conditions, for instance current density, ACD and anode inclination, while the cell voltage was logged, resulting in characteristic voltage data as depicted in Figure 4. Statistical and Fourier analysis of the voltage curves was performed to obtain information regarding the frequency and amplitude of the voltage oscillations, and these data will serve as source for validating the current approach. Measured frequencies of the voltage oscillations were found in the range of 0.22 to 0.73 Hz, with higher frequencies typically observed at higher current density, anode inclination and anode age. Correspondingly, amplitudes were found in the range from 48 to 234 mV, with higher amplitudes typically observed at higher current density, lower anode inclination and younger anodes. Detailed data from the experiments can be found in [12].

Results

The following simulations have all been performed using ANSYS FLUENT R14.5 on a 3D idealized representation of the lab scale electrolysis cell described in [12], as sketched in figure 2. The domain consists of approximately 150k hexahedral cells, with resolution 3x3x1 mm on the anode surface. Transient simulations are performed for 50 seconds flowtime, using a constant time step of 0.001 s. During a typical simulation run, statistically steady conditions were achieved after approximately 30 s. Simulation data from the initial 30 seconds of the simulation

are neglected in the following, focusing only on statistically steady conditions.

Details regarding discretization schemes, solver settings etc. can be found in [8] and [9].

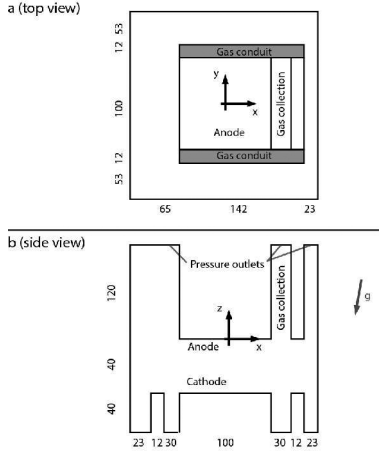


Figure 2: Schematic of simplified computational domain corresponding to [12], numbers indicate dimensions in mm.

Constant surface properties

Initial simulations have been performed considering constant physical parameters, i.e. density, surface tension etc. Chosen physical parameters are assumed to correspond to a bath and CO_2 at 970°C with composition corresponding to the initial specie concentration indicated in table 1.

Six simulations have been performed with conditions corresponding to a sub-set of the experimental conditions described in [12], aiming to capture the main trends of bubble induced voltage oscillations. A summary of the experimental conditions simulated is given in table 2. Case 2 represents an aged anode with an anode profile corresponding to 15 hours electrolysis, while the remaining cases are simulated with sharp corners, as depicted in figure 2.

Table 1: Initial specie concentrations.

Specie	$100Y_i$	Comment
CO_2	0.06	Supersaturation 3, cf. [10]
Al_2O_3	2	Total alumina, 7.7 wt%.
$\text{Na}_2\text{Al}_2\text{O}_2\text{F}_4$	12	Total alumina, 7.7 wt%.
$\text{Na}_2\text{Al}_2\text{OF}_6$	12	Total alumina, 7.7 wt%.
NaF	37.4	
AlF_3	32.6	Excess fluoride 7.8 wt %
Na^+	3.94	

Table 2: Simulated experimental conditions, anode cathode distance (ACD), anode inclination (Inc.), current density (CD) and anode age.

Case (#)	ACD (cm)	Inc. ($^\circ$)	CD A/m^2	Age (h)
1	4	2	0.8	0
2	4	2	0.8	15
3	4	2	0.96	0
4	4	2	1.1	0
5	4	4	0.8	0
6	4	4	0.96	0

A snapshot from a simulation with current density $0.8 \text{ A}/\text{cm}^2$, 4 cm ACD and 2° anode inclination is shown in figure 3. Qualitatively, the depicted topology of the gas bubble layer corresponds well to that observed in recent water model experiments, cf. [11].

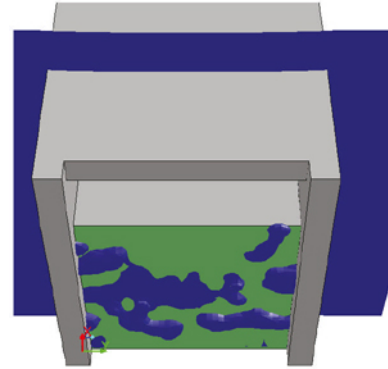


Figure 3: Typical view of simulated gas evolving anode. Gas is shown in blue, while the anode surface is highlighted in green.

Figure 4 shows a comparison between measured and simulated voltage signals, for a current density of $0.8 \text{ A}/\text{cm}^2$, 4 cm ACD and 2° anode inclination.

The frequency and amplitude of the measured signal is found to be 0.435 Hz and 115 mV, while the corresponding numbers obtained from simulations are 0.54 Hz and 97 mV. Considering the full experimental matrix, considering various current densities and anode inclinations, simulations predict frequencies in the range of 0.54 to 0.88 Hz, while amplitudes range from 68 to 135 mV. As for the experiments, higher frequencies are found when increasing the current density, anode age and inclination, while the amplitude increases with increasing current density and reducing the anode inclination. The current simulations do not reveal a strong dependency of anode age upon the amplitude of the signal.

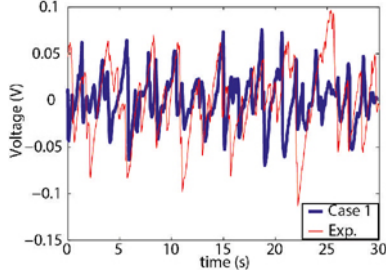


Figure 4: Simulated (blue) and experimental (red) voltage curves for current density 0.8 A/cm^2 , 4 cm ACD and 2° anode inclination.

Simulated results (Amplitude (A) vs. frequency (f)) are compared to the subset of experimental data corresponding to simulated conditions are shown in figure 5, with a least square fit on the form

$$A = \frac{\alpha}{f - \beta} + \gamma, \quad (8)$$

based on the *experimental* data, as proposed by Wang and Taberaux [18]. Evidently, simulated results show overall higher frequencies (i.e. bubble velocities) and lower amplitudes (smaller bubbles), indicating that surface phenomena such as coalescence and adhesion are under predicted in the current simulations. Nevertheless, all simulations are within the expected *range* and follow the experimental trend to an acceptable level.

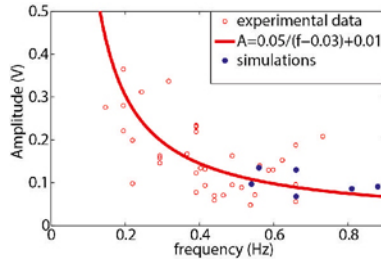


Figure 5: Summary of experiments and simulations under various operating conditions.

The global gas production is shown and compared to that predicted by Faraday's law in figure 6, with excellent comparison, indicating that the reaction schemes proposed by [7] in conjecture with the mass transfer mechanisms proposed by [8] conserve and transfer the CO_2 mass as intended.

Correspondingly, the *global* mass conservation of the bath and its constituents is shown in figure 7 by means of the relative mass deficiency

$$\Delta m_i^* = \frac{m_i(t) - m_i(t=0)}{m_i(t=0)}, \quad (9)$$

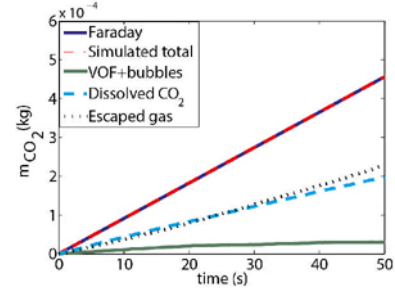


Figure 6: Global mass conservation of gas.

where $m_i(t)$ is the instantaneous mass of field i and $m_i(t=0)$ is the initial value. As seen from figure 7 the total bath mass is conserved. The mass Al_2O_3 is declining due to dissolution, forming $\text{Na}_2\text{Al}_2\text{O}_2\text{F}_4$, while $\text{Na}_2\text{Al}_2\text{OF}_6$, formed by an equilibrium reaction with $\text{Na}_2\text{Al}_2\text{O}_2\text{F}_4$, declines towards equilibrium as CO_2 is produced, as expected, cf. [7] for details.

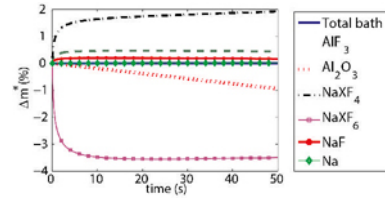


Figure 7: Global conservation of bath and species.

Variable surface properties

As seen from figure 7, the *global* composition of the bath does not change significantly from the initial conditions, due to the relatively short simulation times considered (50 s flow time in total, compared to several thousand seconds in [7]). From a *global* perspective, it is thus not expected that the bath properties will change considerably either. However, local concentration changes due to bubble formation and screening could in principle influence the overall voltage behavior of the cell.

The voltage curve resulting from a simulation with conditions corresponding to case 1 (cf. table 2), but with composition dependent surface tension and contact angle is shown in figure 8 and compared to the case where the properties are constant (case 1). The resulting frequency and amplitude of the full simulation is 0.29 Hz and 150 mV , respectively, thus apparently bringing simulations closer to the range measured experimentally.

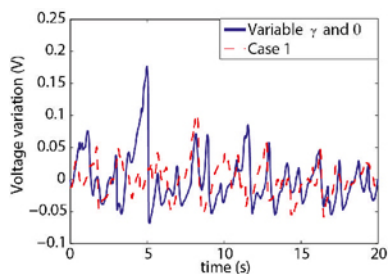


Figure 8: Voltage curve with composition dependent surface tension and contact angle.

Summary and conclusions

A multiscale and -field model for anodic bubble flow allowing for bath chemistry and variable bath properties has been presented. Results have been verified by comparison to lab scale electrolysis experiments, showing good correspondence, simultaneously illustrating the complexity and sensitivity of detailed anodic bubble flow simulations.

Future work will focus on extending the analysis to a full scale anode, thus enabling a virtual flow lab.

Acknowledgments

The present work has been performed in the project “Gas and Alumina Distribution and Transport” (GADT), financed by the Research Council of Norway and Hydro Primary Metal Technology. Permission to publish the results is gratefully acknowledged.

References

- [1] B.P. Moxnes, et al. *Improved cell operation by redistribution of the alumina feeding*, Light Metals 2009, pp. 461-466.
- [2] V. Gusberti, et al. *Modeling the mass and energy balance of different aluminium smelting cell technologies*, Light Metals 2012, pp. 929-934.
- [3] Y.Q. Feng, M. Cooksey, M.P. Schwarz, *CFD Modelling of alumina mixing in aluminium reduction cells*, Light Metals 2010, pp. 455-460.
- [4] Y.Q. Feng, et al. *Development of Bubble Driven Flow CFD Model Applied for Aluminium Smelting Cells*, J. Comp. Multiphase Flows, Vol. 2:3, 2010, pp. 179-188.
- [5] Y.Q. Feng, M. Cooksey, M.P. Schwarz, *CFD Modelling of alumina mixing in aluminium reduction cells*, Light Metals 2011, pp. 543-548.
- [6] P.J. Witt, et al. *Modelling bubble flow with CFX and Fluent for aluminium reductions cells*, 9th Int. Conference on CFD in the Mineral and Process Industries, CSIRO, Melbourne, Australia, 10-12 Dec, 2012.
- [7] P.J. Witt, et al. *A Six Chemical Species CFD Model of Alumina Reduction in a Hall-Héroult Cell*, 10th Int. Conference on CFD in the Oil & Gas, Metallurgical and Process Industries, SINTEF, Trondheim, Norway, 17-19 June, 2014.
- [8] K.E. Einarsrud, *A Treatise On Interpolat Transport Phenomena*, PhD Thesis 201. NTNU: Trondheim, Norway, 2012.
- [9] K.E. Einarsrud, S.T. Johansen, *Modelling of Bubble Behaviour in Aluminium Reduction Cells*, Progress in Computational Fluid Dynamics, Vol. 12:2, 2012.
- [10] K.E. Einarsrud, S.T. Johansen, I. Eick, *Anodic bubble behavior in Hall-Héroult cells*, Light Metals 2012, pp. 875-880.
- [11] A. Simonsen, K.E. Einarsrud, I. Eick, *The Impact of Bubble-Bubble Interactions on Anodic Gas Release: A Water Model Analysis*, Light Metals 2015, pp. -.
- [12] I. Eick, et al. *Voltage and Bubble release behaviour in a laboratory cell at low anode-cathode distance*, 10th AASTC, Launceston, Tasmania, 2011.
- [13] B. Lafaurie, et al. *Modelling Merging and Fragmentation in Multiphase Floes with SURFER*, Journal of Computational Physics, Vol. 113:1, pp. 134-147, 1994.
- [14] T.H. Shih, et al. *A new $k-\epsilon$ Eddy-Viscosity Model for High Reynolds Number Turbulent Flows - Model development and Validation*, Computers & Fluids, Vol. 24, pp. 227-238, 1995.
- [15] Thonstad et al., *Aluminium electrolysis: fundamentals of the Hall-Héroult process*, Aluminium-Verlag, 2003.
- [16] R.C. Dorward, *Reaction Between Aluminum and Graphite in the Presence of Cryolite*, Metallurgical Transactions, Vol. 4, pp. 386-388, 1973.
- [17] ANSYS, www.ansys.com
- [18] X. Wang and A.T. Taberaux, *Anodic phenomena - Observations of anode overvoltage and gas bubbling during aluminium electrolysis*, Light Metals 2000, pp. 239-247.